Cell

Leading Edge
Review

Clarifying Tissue Clearing

Douglas S. Richardson[1,2,*] and Jeff W. Lichtman[1,2,3,*]
[1]Harvard Center for Biological Imaging
[2]Department of Molecular and Cellular Biology
[3]Center for Brain Science
Harvard University, Cambridge, MA 02138, USA
*Correspondence: drichardson@fas.harvard.edu (D.S.R.), jeff@mcb.harvard.edu (J.W.L.)

http://dx.doi.org/10.1016/j.cell.2015.06.067

Biological specimens are intrinsically three dimensional; however, because of the obscuring effects of light scatter, imaging deep into a tissue volume is problematic. Although efforts to eliminate the scatter by "clearing" the tissue have been ongoing for over a century, there have been a large number of recent innovations. This Review introduces the physical basis for light scatter in tissue, describes the mechanisms underlying various clearing techniques, and discusses several of the major advances in light microscopy for imaging cleared tissue.

Challenges and Approaches to Imaging Thick Tissues

Biologists have long appreciated that it is easier to see things in thin sections than thick volumes—hence, the pervasive use of microtomes, the indispensable tools that cut thin sections of tissue samples and provide information about cellular constituents within two-dimensional sections of biological tissues. Now, however, there is a growing trend to inquire about structure in three dimensions, requiring biologists to contend with volumes rather than sections. The need for volumetric imaging is related to the inherent three-dimensional structure of cells and organs. The nervous system is the most obvious example, given that most individual neurons extend in many directions and their true nature cannot be ascertained by a thin section. Also, much of developmental biology requires understanding morphogenesis of organs and even whole animals in the context of three dimensions. How does one obtain such three-dimensional information? One possibility is to reconstruct three-dimensional information by putting into register a series of serial thin sections. This approach is technically challenging due to loss or distortion of individual sections that become torn, folded, compressed, or stretched. With imperfect sections, the final volumetric reconstruction can be unsatisfactory. However, if done under sufficient control, serial sectioning can give rise to very useful results (Oh et al., 2014; Toga et al., 1997). Another possibility is to image the surface of a block of tissue and then sequentially shave off the surface. Such "blockface" methods are used in both light (Toga et al., 1994; Tsai et al., 2009a) and electron microscopy (Denk and Horstmann, 2004; Ichimura et al., 2015). Blockface approaches eliminate the loss and alignment issues of sections but are destructive in the sense that, once each section is imaged, it is destroyed to reveal the next block surface. The other possibility is to image the volume without sectioning. Non-sectioning approaches avoid the demanding alignment issues, and the same tissue sample in principle can be imaged multiple times. One problem, however, with imaging a volume is that out of focus information from regions above and below the plane of focus contaminates information from any one plane. This problem led Marvin Minsky to invent the first confocal microscope to filter the out-of-focus light (Minsky, 1988) and led to the revolution of "optical sectioning" techniques—most notably, commercial laser-scanning confocal microscopes, laser scanning two-photon microscopy, parallelized confocal (i.e., spinning disk), computational image deconvolution methods, and light-sheet approaches (reviewed in Conchello and Lichtman, 2005; Mertz, 2011; Reynaud et al., 2008). All of these microscopy methods provide information about single planes of a volume by minimizing contributions from other parts of the volume and do so without physical sectioning. These methods thus allow access to image data from any arbitrary thin section in a thick sample. By creating a "stack" of such optically sectioned images, a full reconstruction of the three-dimensional features of a tissue volume can be ascertained.

But even with the advent of optical sectioning microcopies, there remain major obstacles facing a microscopist looking at biological tissues that are thick. First, in some tissues, a pigment gives the tissue a color (Box 1). Second, inherently fluorescent molecules may be present in the tissue or introduced during processing, giving rise to autofluorescence that masks fluorescently labeled structures of interest (Box 2). The final problem, and the one that we focus on here, is that most biological tissues have an intrinsic milky appearance. This property gives tissues the look of frosted glass or translucence. The lack of clarity undermines sharp images and becomes progressively more of an impediment the deeper one tries to look into a tissue volume.

This translucency is caused by light scattering. Light rays that should travel in straight lines are deviated many times as light is reflected off of molecules, membranes, organelles, and cells in the tissue. It is useful to delve a bit into the underlying physics of scattering in order to understand the kinds of strategies that have been used to clear tissues.

How Does Tissue Scatter Light?

The purpose of this short analysis is to understand that clearing tissues is not aimed at preventing scattering (only a vacuum has no scattering) but, rather, assuring that there is a high uniform

Box 1. Limiting Absorption

Absorption of light within a sample can limit both the excitation light entering a tissue and the fluorescence emission returning to the detector. Hemoglobin, myoglobin, and melanin are the primary molecules that are responsible for visible light absorption in biological tissue. Hemoglobin is present in all vertebrate species (except the crocodile ice fish) and in many invertebrates. Hemoglobin containing red blood cells can be removed from vertebrates by perfusion of clear buffer through the circulatory system. When perfusion is not an option, treating the specimen with hydrogen peroxide to decolor hemoglobin or amino alcohol in a basic solution to elute the heme group is a possibility (Tainaka et al., 2014). Hydrogen peroxide, however, is potentially damaging to tissue structure and may adversely affect fluorescent protein emission (Alnuami et al., 2008; Steinke and Wolff, 2001). Myoglobin, the colored pigment in skeletal muscle, is also decolored by these same two treatments. Melanin, the primary pigment in hair and skin, can be avoided in albino mutant animals. In zebrafish, chemical treatment with 1-phenyl-2-thiourea or genetic modifications (the *casper* mutant) can be used to block the synthesis of melanin or the development of pigmented melanocytes (White et al., 2008). One final option is to move to an area of the electromagnetic spectrum in which biological tissue does not absorb. Often referred to as the “near-infrared window,” light with wavelengths of 650–1,350 nm is very weakly absorbed by biological tissues and can be used with near IR fluorophores or two-photon microscopy. A second imaging window, in the range of 1.3–1.4 μm has recently been identified and used to image >2 mm into tissue, even passing through bone (Hong et al., 2014). Unfortunately, none of these techniques address the primary hindrance to deep tissue imaging, the scatter of light in biological tissue.

Box 2. Autofluorescence

Autofluorescence is the background glow that results from excitation of either inherently fluorescent molecules in a sample or those introduced into the sample during its preparation. Typically, the broadband glow decreases image quality by lowering the signal-to-noise ratio across multiple fluorescence channels. Autofluorescence may arise from endogenous fluorescent biomolecules (NADPH, collagen, flavins, tyrosine, and others) or may be introduced by the formation of Schiffs bases during fixation with aldehydes (glutaraldehyde is worse than paraformaldehyde). A number of techniques reduce autofluorescence somewhat, including: bleaching with high-intensity lighting (Duong and Han, 2013), sodium borohydride treatment to eliminate Schiffs bases (Clancy and Cauller, 1998), and spectral unmixing to remove broadband fluorescent signals (Zimmermann, 2005). It is important to remember that background autofluorescence is not necessarily removed by tissue clearing methods.

density of scatterers so that lateral scattering is minimal and that all wavelengths of light pass “through” the tissue.

The ways to think about light range from light as rays, light as waves, or light as photons. Although rays are easiest to talk about and photons seem closest to the true essence of light, it is the wave framework that is most helpful when thinking about light scattering. Light waves of a particular color (wavelength) vibrate at a particular frequency and have an electrical and magnetic component. The electrical component is the one that for the most part interacts with the atoms in biological tissues. The wave vibration is extraordinarily fast. For example, red light (600 nm wavelength) vibrates at the rate of 0.5×10^{15} oscillations per second. Let’s imagine this wave is a plane that passes an atom or molecule from a particular direction (plane waves are basically light that propagates in a single direction without converging or diverging, like a laser beam). As the plane wave reaches the atoms, it may impart some of its energy from its electrical component to the atom or molecule, typically to an outer electron which is more susceptible to absorbing energy than electrons closer to the nucleus or protons or neutrons in the nucleus. For most molecules, the energy absorbed by an electron is not sufficient to cause an electron to jump to a new orbital. Therefore, neither fluorescence (re-emission of lower-energy light; Lichtman and Conchello, 2005) nor ionization (removal of the electron from the atom or molecule) occurs. Rather, the light wave’s vibrational energy momentarily causes the electron to vibrate (as if it were connected to its nucleus by a spring that was stretched a bit by the incoming light wave). The electron vibration is short lived, and all of the energy absorbed is quickly released again in the form of another light wave. There are a few differences between the incoming light wave and the outgoing light wave emitted by the atom or molecule. First, the incident light is coming from a particular direction, but the outgoing light is sent in all directions as a spherical wave (see below). Thus, the light is scattered. Because the whole process occurs without any energy loss, the light is said to be elastically scattered. Elastic scattering means that the vibrational frequency (and hence the wavelength) of the scattered light is unchanged from the incoming light. The second difference is that the interaction between the incident light wave and the electron cloud of the scatterer, although brief, causes a momentary pause in the light’s progression, evidenced by the fact that the new scattered wave is delayed (usually one-half of a wavelength). The duration of the delay is only about a femtosecond (10^{-15} s) for visible light. But as light passes through a material, it interacts with many molecules and these little delays associated with each interaction add up. As a result, light’s propagation through the material is slowed down. This reduced velocity is the basis of the so-called refractive index of the medium (literally, the ratio of the speed of light in a vacuum divided by the speed of light in the medium). The amount of slowdown per unit volume is proportional to the density of molecules and hence the number of electrons that the light wave can interact with. But density is only one variable that affects refractive index. Some materials such as the hydrophobic molecules in the plasma membrane have electrons that are more susceptible to absorbing light energy than other molecules, such as the hydrogen atoms in water. Thus, even though the density of water surrounding a cell is higher than the density of the fatty material in cell membranes (fat, after all, floats in water), the membrane has a higher index of refraction than water (1.45 versus 1.33).

Although it is commonly explained that scattering occurs due to the mismatch of the index of refractions at interfaces between different substances in a tissue, this is not the whole story. As we will explain below, scattering occurs everywhere that there are

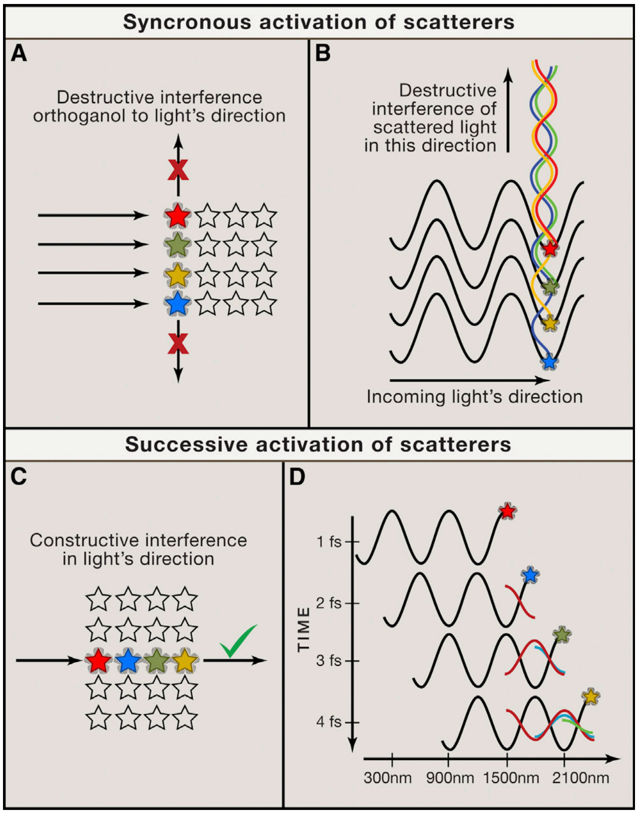
Syncronous activation of scatterers
A
Destructive interference orthoganol to light's direction
B
Destructive interference of scattered light in this direction
Incoming light's direction
Successive activation of scatterers
C
Constructive interference in light's direction
D
1 fs
2 fs
3 fs
4 fs
TIME
300nm
900nm
1500nm
2100nm

Figure 1. Wave Optic View of Light Passing through a Homogenous Scattering Medium

(A) In a material with a uniform density of scattering molecules (shown here as stars) such as glass, water, or air, light is not scattered orthogonal to the direction of the incoming light wave (arrows). In this situation, all of the scattering molecules that are excited simultaneously (colored stars) are aligned orthogonal to the direction of the plane wave.

(B) A wave view to explain what is happening in (A). Each of these simultaneously excited molecules generate wave energy in all directions, but by virtue of their different positions, there is for each wave always another wave that is exactly half a wavelength out of phase with it in the vertical direction, causing destructive interference.

(C) The scatters that are aligned in the direction of the incoming light wave (arrow) are activated sequentially (colored stars). Their excitations sum constructively in the forward direction, causing no attenuation of the light moving through the medium.

(D) A wave view to explain what is happening in (C). Shown is the same light wave at four successive time points 1 fs apart. At the first time point (top), the wave imparts vibrational energy to a scattering molecule (red star). 1 fs later, the molecule emits the absorbed energy (red wave, half-phase delay from incoming light). At this time, another molecule (blue star) is first excited by the incoming light wave. At 2 fs, the molecule denoted by the blue star emits its scattered light (blue wave) that is in phase with the scattered light from the red wave, and a third molecule (green star) is excited by the incoming light wave. At 3 fs, the light from all three scatters is vibrating in phase (superimposition of the red, blue, and green waves) and another molecule (yellow star) absorbs energy from the incoming light wave. In this way, all forward moving scattered light remains in phase, causing no attenuation in light energy in this direction.

molecules, not just at sites of refractive index mismatches. It is more accurate to say that heterogeneity in the amount of scattering between different regions in biological material is actually what gives rise to the scattering and milky appearance.

The light energy absorbed by an electron is re-radiated in all directions as an expanding spherical wave. This spherical wave, sometimes called a "wavelet," is a wave that diverges from a source as if that source were a luminous object sending wave energy along the expanding surface of a sphere. The two-dimensional analog of a spherical wave would be the circular wave that originates on the surface of a pool of water from the site where a pebble is dropped. The emitted spherical wave, just like the original incident light, can and will interact with electrons in other atoms or molecules re-emerging over and over again as new spherical waves at different sites. The wave conception of light is powerful because it explains how light waves can add their amplitudes and give rise to brighter light though constructive interference when they crest or trough in phase. The intensity of light is actually the square of the summed amplitudes integrated over time, so both troughs and crests give light energy. The wave conception also explains why light may sometimes not be present if two waves reach the same place half a wavelength out of phase (i.e., while one wave is in the crest and another is in the trough at the same place). In this situation, the sum of their amplitudes is zero, and no light from those wavelets can appear at that site; this is known as destructive interference.

Destructive interference explains why homogenous materials, such as air, water, and glass, appear clear even though the molecules in these substances are scattering light. In such materials, the density of scattering molecules is so high that many scatterers exist even over dimensions much smaller than the wavelength of visible light (i.e., between 400 and 700 nm). Air molecules, for example, are about 3 nm apart, and liquid water molecules are about ten times closer together (Hecht, 2001). When a plane wave of light passes through such materials, all of the molecules in a plane are set into vibration simultaneously and give rise to densely packed spherical waves. The consequence of such a high density of scatterers is nearly complete destructive interference in the axes of the plane (Figures 1A and 1B). This cancellation occurs because when wavelets are uniformly distributed at high density, each point in the plane is bombarded by wavelets at every phase. For example, for every cresting wave, another is in the trough at the same place. As a result, the sum amplitude is zero in the plane, preventing any light from escaping in any lateral direction out of the plane (i.e., hardly any light propagates perpendicular to the direction of the impinging light wave; Figure 1B). We know, of course, that light continues in the forward direction in media like air, water, or glass without difficulty, raising the question of why the scatterers in front of each molecule don't also give rise to destructive interference by the same argument. Distinct from the simultaneous vibrations of all the scatterers in a plane, the molecules in front of the plane are activated later, when the primary plane wave reaches them (Figures 1C and 1D). The scattered light from the molecules that were previously acted on by the plane wave reach this forward direction slightly later due to the additional half-wavelength phase delay of scattered light. The scattered light from the earlier illuminated molecules always (!) constructively interferes with the scattered light originating from molecules at more forward sites (Figure 1D). Thus, in the forward direction, the amplitudes sum constructively and light propagates.

Given that dense materials like water don't scatter in lateral directions, why do dense cellular tissues scatter? The important point here is the inhomogeneity of scatterers. The prevention of lateral scattering requires that each scattering molecule is equidistant from other scatterers at every distance in the plane. For example, in living tissue, a physiological saline solution surrounds the membrane of a cell. This means that the amount of scattering in the membrane is likely to be different than the amount of scattering in the saline solution. Thus, scattering from the water molecules near the membrane may not be completely cancelled by the scattering from the membrane itself; thus, both materials will generate light scattered perpendicular to the direction of light impinging on the sample.

If a tissue is sufficiently thick, then most of the incoming light will be scattered and the tissue will behave as if it contains a multitude of little luminous sources, each sending light in every direction. This multiple scattering is the property that generates the whitish translucency of tissues. The whitish color implies that all wavelengths of visible light are scattered, and this is due to the intrinsic inhomogeneities of scatterers in the tissue.

The sizes of the inhomogeneities affect the wavelength of the light that is scattered. For particles that are much smaller than the wavelength of visible light, short-wavelength light has a greater probability of being absorbed and re-emitted (in proportion to the wavelength to the fourth power, Rayleigh scattering). As a result, there is some tendency for short wavelengths to scatter more than long ones. This is sometimes mentioned as an advantage of using the long-wavelength infrared-light-based two-photon excitation on thick samples, as relatively less of the exciting light is scattered compared to visible or ultraviolet light. For particles larger than about one-tenth of the wavelength, such as organelles and large protein complexes, the wavelength dependence of scattering is not evident (Mie scattering).

Older Clearing Techniques

It has been known for more than a century that biological samples can be stably maintained in a somewhat transparent hardened material resin. Indeed, ancient flies in amber show that resins can stably maintain biological samples for 50 million years. Many of the resins used by biologists are hydrophobic, requiring that the sample be dehydrated. Following dehydration (in a series of alcohol-water mixtures with progressively less water), samples are put into solvents that dissolve lipids and act to remove one of the main sites of tissue inhomogeneity: the membranes. Canada Balsam is such a resin that provides a transparent mountant for tissue that is dehydrated and cleared with xylene. Such resins, however, are intrinsically fluorescent and are best used with absorbance dyes like the Golgi stain rather than fluorophores due to high background (Rost, 1992). Moreover, most fluorescent proteins require an aqueous environment, so this kind of clearing quenches the signal.

At the beginning of the 20th century, Spalteholz described a clearing technique for large (entire organ and organ system) tissues using organic solvents (Spalteholz, 1914). The method was intensive, requiring various dehydration, tissue bleaching, and clearing steps. However, it produced samples that were unprecedented at the time and helped to push forward the field of anatomy (Spalteholz, 1898). Unfortunately, this approach damaged the superficial few centimeters of a tissue and therefore was useful only for clearing the largest samples (Steinke and Wolff, 2001).

Modern Clearing Techniques

The optical sectioning advances mentioned above (i.e., confocal, two-photon, and image deconvolution) led to fluorescence volume imaging becoming the contrast method of choice for microscopy at the end of the 20th century. Most notably, two-photon detection pushed microscopy from imaging depths of tens of microns to fractions of a millimeter (Denk et al., 1990). Genetically encoded fluorescent proteins provided a labeling method with high specificity that did not require antibodies to diffuse through the entire sample to their target and hence motivated ever deeper imaging (Chalfie et al., 1994). However, the scatter of light in heterogeneous tissue remained a limiting factor for these techniques, preventing researchers from achieving high-resolution three-dimensional renderings of thick tissue. The source of the scattering is a diverse set of cellular constituents, including ribosomes, nuclei, nucleoli, mitochondria, lipid droplets, membranes, myelin, cytoskeletal components, and extracellular matrix components such as collagen and elastin. Therefore, techniques that can alter the scattering properties of cellular components hold the key for unlocking the full potential of today's best optical sectioning light microscopes.

As volume fluorescence microscopy gained in popularity and advances in data acquisition and storage made large volume imaging possible, a number of attempts were made to revisit the tissue clearing techniques that had originally been developed by Spalteholz. All tissue clearing techniques focus on equilibrating the refractive index throughout a sample to reduce inhomogeneities in light scatter. However, the field was quickly split into two approaches: (1) those that followed Spalteholz's historical reliance on tissue dehydration and solvent-based clearing and (2) emerging aqueous-based techniques (Table 1).

Solvent-Based Clearing

Solvent-based clearing techniques are most commonly comprised of two steps: (1) dehydration with lipid solvation and (2) additional lipid solvation and clearing by refractive index matching to the remaining dehydrated tissue's index (Figure 2A).

A number of solvents have been tested for use in either the dehydration or clearing steps (Becker et al., 2012; Peters, 1961). Most commonly, dehydration is now performed using methanol with or without hexane or with tetrahydrofurane (THF) alone (Becker et al., 2012; Dodt et al., 2007; Ertürk et al., 2012a, 2012b; Renier et al., 2014; Spalteholz, 1914). While these agents remove water, they also solvate and remove some of the lipids. Removal of water and lipid results in a fairly homogenous, primarily proteinaceous, dense (i.e., high index of refraction) sample. Dehydrated protein has a refractive index of >1.5 (higher than water or lipid). Therefore, the dehydration step must be followed by a second set of agents that solvate additional lipid and intercalate homogeneously throughout the sample to clear it by matching the higher refractive index of the defatted and dehydrated tissue. To date, methylsalicilate, benzyl alcohol, benzyl benzoate, dichloromethane, and dibenzyl ether have been used as final clearing solutions (Becker et al., 2012; Dodt et al., 2007; Ertürk et al., 2012a, 2012b; Renier et al., 2014; Spalteholz, 1914; Steinke and Wolff, 2001).

The ideal organic solvent for clearing possesses two characteristics. First, it must have a high lipid-solvating capacity and,

Table 1. Comparison of Clearing Techniques

Solvent Based	Final RI	Key Components	Time to Clear	Immunostaining Demonstrated	Alterations in Tissue Morphology	FP Emission	Detergent Used	Lipid Preserved	Electrophoresis	Hydrogel Embedding	Clearing Solution Perfused	Toxic	Reference
Spatleholz	1.55	benzylbenzoate/ methylsalicilate	months	no	shrinkage	no	no	no	no	no	no	yes	Spalteholz 1914
BABB	1.55	benzylalcohol/ benzylbenzoate	days	yes	shrinkage	yes, but only half day	no	no	no	no	no	yes	Dodt et al., 2007
3DISCO	1.56	dichloromethane/ dibenzylether	hours–days	limited	shrinkage	yes, but only 1–2 days	no	no	no	no	no	no (DBE)	Ertürk et al., 2012a, 2012b
iDISCO	1.56	dichloromethane/ dibenzylether	hours–days	yes	shrinkage	yes, but only 2–4 days	no	no	no	no	no	no (DBE)	Renier et al., 2014

Simple Immersion	Final Refractive Index	Key Components	Time to Clear	Immunostaining Demonstrated	Alterations in Tissue Morphology	FP Emission	Detergent Used	Lipid Preserved	Electrophoresis	Hydrogel Embedding	Clearing Solution Perfused	Toxic	Reference
Sucrose	1.44	sucrose	1 day	yes	Shrinkage	yes	Triton (2%)	no	no	no	no	no	Tsai et al., 2009b
FocusClear	1.47	diatrizoic acid	hours–days	yes	no	yes	Tween 20	yes	no	no	no	no	Chiang et al., 2002
ClearT[a]	1.44	formamide	hours–days	yes	no	no	no	yes	no	no	no	no	Kuwajima et al., 2013
ClearT2[a]	1.44	formamide/PEG	hours–days	yes	no	yes	no	yes	no	no	no	no	Kuwajima et al., 2013
SeeDB	1.48	fructose/ thioglycerol	days	no	no	yes	no	yes	no	no	no	no	Ke et al., 2013
FRUIT[a]	1.48	fructose/ thioglycerol/urea	days	no	minimal expansion	yes	no	yes	no	no	yes	no	Hou et al., 2015
TDE[b]	1.42	2,2′-thiodiethanol	days–weeks	yes	no	yes	8% SDS (optional)	no	optional	optional	no	no	Costantini et al., 2015; Aoyagi et al., 2015; Staudt et al., 2007

Hyperhydration	Final Refractive Index	Key Components	Time to Clear	Immunostaining Demonstrated	Alterations in Tissue Morphology	FP Emission	Detergent Used	Lipid Preserved	Electrophoresis	Hydrogel Embedding	Clearing Solution Perfused	Toxic	Reference
Sca*l*e A2	1.38	4M urea, 10% glycerol	weeks	no	expansion	yes	Triton X-100 (0.1%)	no	no	no	no	no	Hama et al., 2011
Sca*l*e U2	1.38	4M urea, 30% glycerol	months	no	no	yes	Triton X-100 (0.1%)	no	no	no	no	no	Hama et al., 2011

(*Continued on next page*)

Table 1. Continued

CUBIC	CUBIC1, 1.38; CUBIC2, 1.48	4M urea/50% sucrose	days	yes	expansion	yes	Triton X-100 (50%)	no	no	no	no	no	Susaki et al., 2014
Whole-Body CUBIC	1.38	4M urea	days	yes	expansion	yes	Triton X-100 (10%)	no	no	no	yes	no	Tainaka et al., 2014
Hydrogel Embedding	Final Refractive Index	Key Components	Time to Clear	Immunostaining Demonstrated	Alterations in Tissue Morphology	FP Emission	Detergent Used	Lipid Preserved	Electrophoresis	Hydrogel Embedding	Clearing Solution Perfused	Toxic	Reference
CLARITY	1.45	FocusClear/80% glycerol	days	yes	slight expansion	yes	SDS (8%)	no	yes	yes	no	no	Chung et al., 2013
PACT	1.38–1.48	Histodenz	days–weeks	yes	slight expansion	yes	SDS (8%)	no	no	yes	no	no	Yang et al., 2014
PARS	1.38–1.48	Histodenz	days	yes	no	yes	SDS (8%)	no	yes	yes	yes	no	Yang et al., 2014

RI, refractive index; FP, fluorescent protein.

[a]Denotes techniques that also have a Hyperhydration component.

[b]Can be combined with CLARTIY/PACT/PARS

second, it must possess a high (≥1.5) refractive index. As alluded to above, low-density organic molecules can have surprisingly high refractive indices if a number of loosely held electrons, such as those found in the pi bonds of an aromatic ring, are present. Many of the most successful clearing solvents contain one or two aromatic rings in their structures (Figure 2). Oscillations can easily be imparted to these electrons when they are placed in the electric field of a light wave. When the clearing solvent's refractive index is well matched to the refractive index of the dehydrated tissue sample, all non-forward scatter is destructive, as described above, and the tissue becomes clear. Importantly, these ring structures do not generally allow for electrons to be promoted to excited states and yield fluorescence with the moderate energy levels available at visible light wavelengths.

One major limitation to solvent-based clearing methods is that dehydration removes water molecules from the sample that are necessary to maintain emission from most fluorescent protein chromophores. This limitation was partially addressed in two of the most recent advances in solvent clearing, 3DISCO (Ertürk et al., 2012a, 2012b) and iDISCO (Renier et al., 2014). These techniques allow for solvent-based clearing that can maintain fluorescent protein emission for a few days. 3DISCO replaces the methanol dehydration step with incubation in THF. iDISCO presents two options. First, a traditional methanol dehydration step can be performed that results in the quenching of fluorescent proteins. These molecules are then visualized by standard immunofluorescence with an antibody directed against the fluorescent protein. The second approach involves replacing the methanol dehydration step with a number of aqueous solutions containing phosphate-buffered saline (PBS), detergent, and dimethyl sulfoxide (DMSO). This combination of aqueous solutions and solvents sustained GFP expression longer than the traditional BABB or 3DISCO protocols, presumably due to residual water in the sample; however, by 2–4 days, the fluorescence had dissipated. Alternative labeling options include fluorescent proteins optimized for correlative electron and light microscopy that are able to survive dehydration (Paez-Segala et al., 2015) or the use of immunofluorescent labeling with antibodies raised against the fluorescent proteins and conjugated to dehydration-resistant organic dyes (Cai et al., 2013; Renier et al., 2014).

The solvent-based clearing techniques are robust and work on a number of different tissue types. However, the toxic nature of many solvents, their capacity to dissolve glues used in the construction of objective lenses, substantial shrinkage of tissue during dehydration (up to 50%; Becker et al., 2012), and the quenching of fluorescent protein emission reduce their utility.

Aqueous-Based Clearing

The inability to preserve fluorescent protein emission in many of the solvent-based techniques and a desire to prevent changes in tissue architecture (primarily dehydration-induced shrinkage) led a number of researchers to pursue aqueous-based clearing solutions. All aqueous-based techniques to date utilize one of three mechanistic approaches for homogenizing the scattering throughout a sample: (1) passive immersion in a solution that is

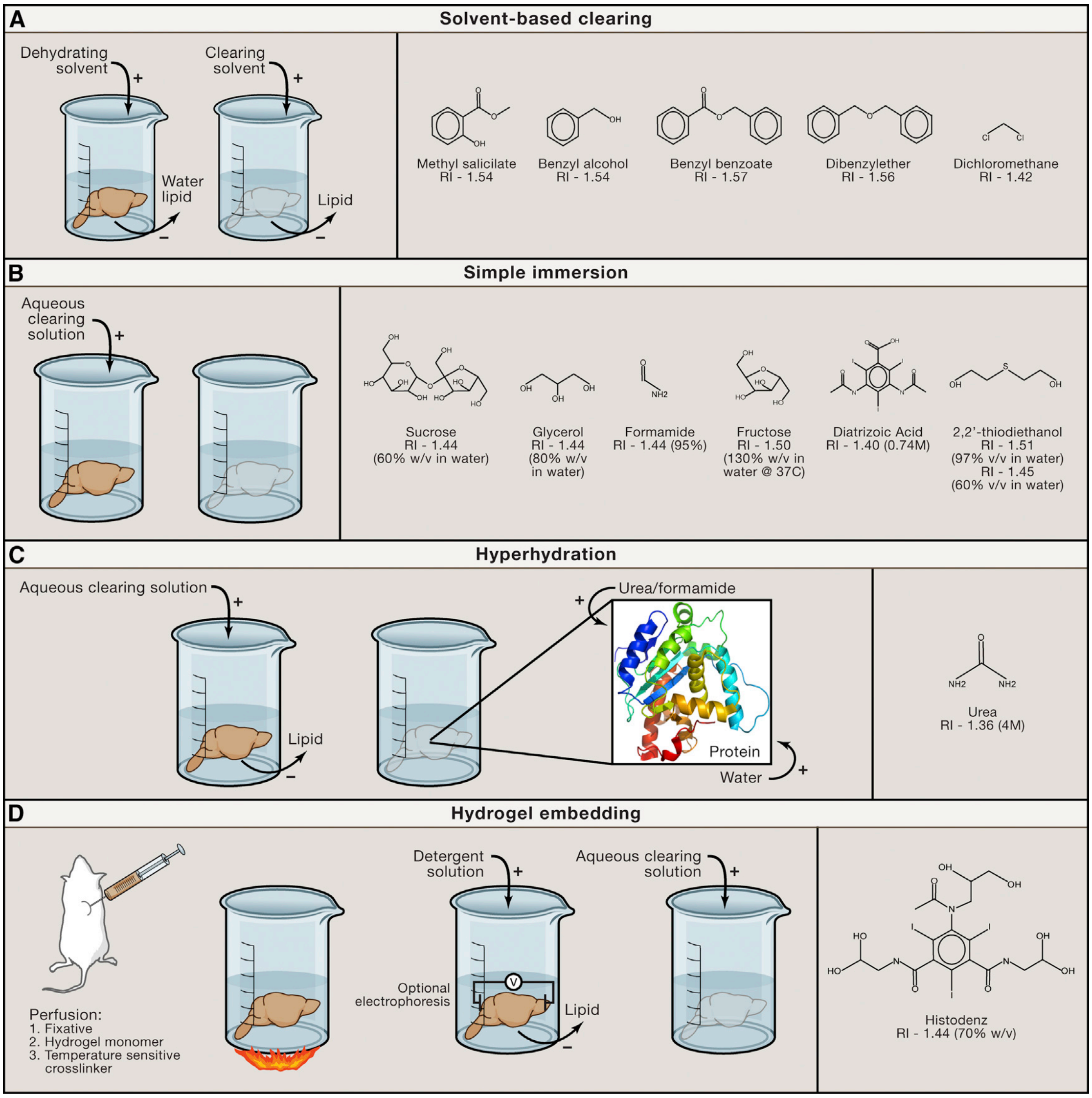
A
Solvent-based clearing
Dehydrating solvent
+
Clearing solvent
+
Water lipid
−
Lipid
−
Methyl salicilate RI - 1.54
Benzyl alcohol RI - 1.54
Benzyl benzoate RI - 1.57
Dibenzylether RI - 1.56
Dichloromethane RI - 1.42
B
Simple immersion
Aqueous clearing solution
+
Sucrose RI - 1.44 (60% w/v in water)
Glycerol RI - 1.44 (80% w/v in water)
Formamide RI - 1.44 (95%)
Fructose RI - 1.50 (130% w/v in water @ 37C)
Diatrizoic Acid RI - 1.40 (0.74M)
2,2'-thiodiethanol RI - 1.51 (97% v/v in water) RI - 1.45 (60% v/v in water)
C
Hyperhydration
Aqueous clearing solution
+
Lipid
−
Urea/formamide
+
Protein
Water
+
Urea RI - 1.36 (4M)
D
Hydrogel embedding
Perfusion:
1. Fixative
2. Hydrogel monomer
3. Temperature sensitive crosslinker
Detergent solution
+
Optional electrophoresis
V
Lipid
−
Aqueous clearing solution
+
Histodenz RI - 1.44 (70% w/v)

Figure 2. Methodology of Tissue Clearing Techniques

(A) (Left) Solvent-based clearing is a two-step process. First, the tissue is dehydrated and lipid is removed. Second, the tissue is moved to a high refractive index solvent where additional lipid solvation and clearing occurs. (Right) Molecules commonly used for solvent-based clearing along with the refractive indices (RI) of the pure chemical.

(B) (Left) For simple immersion, the tissue to be cleared is placed in an aqueous clearing solution for days to months. During this time, the solution is exchanged repeatedly. (Right) Molecules commonly used for simple immersion along with the refractive indices (RI) at the commonly used concentration.

(C) Hyperhydration involves submerging the sample in an aqueous solution and allowing it to passively clear. During this clearing step, urea or formamide in the clearing solution can enter tightly folded regions of high refractive index proteins, creating an osmotic gradient that pulls in water as well. This partially denatures the protein, hydrates it, and decreases its overall refractive index. Some hyperhydration methods contain detergent that is used to disrupt membranes and remove lipid from the sample.

(D) (Left) Hydrogel embedding is most often performed on an entire animal by perfusing with a fixative, a temperature-sensitive crosslinker, and the hydrogel monomer. Alternatively, these chemicals can be passively diffused into an isolated tissue sample. Once fixed, the tissue of interest is warmed to induce hydrogel crosslinking. The sample is then placed in a detergent solution to remove lipid material passively or via an electrophoretic charge. Finally, the lipid-free sample is placed in a high refractive index matching solution for clearing. Histodenz is one high refractive index molecule that can be a component of this clearing solution. Glycerol, TDE, or diatrizoic acid also can play this role.

refractive index matched to the tissue, (2) removal of lipid followed by hydration of the sample to lower the refractive index of the remaining tissue components or, (3) active or passive removal of lipid followed by immersion in a refractive index matched medium.

Simple Immersion

Passive clearing by immersion in high refractive index solutions is effective especially for smaller samples. Most commercially available microscopy mounting media are glycerol based with refractive indices between 1.40 and 1.44 and are able to impart a slight clearing effect on thin cells and tissues. However, because the refractive index of these mountants are not well matched to that of coverslip glass and immersion oil (1.51), reduced image quality due to spherical aberration is often noticeable in samples greater than a few cell layers thick, and additional clearing and/or index-matching approaches are required (Staudt et al., 2007).

In simple immersion, a tissue sample is placed in an aqueous solution containing a dissolved, high refractive index molecule (Figures 2B) and is allowed to gradually clear. Sucrose (Tsai et al., 2009b), fructose (Costantini et al., 2015; Ke et al., 2013), glycerol (Meglinski et al., 2002), 2,2′-thiodiethanol (TDE) (Aoyagi et al., 2015; Hou et al., 2015; Staudt et al., 2007), and formamide (Kuwajima et al., 2013) have all been used for this purpose. Generally, a refractive index greater than 1.45 needs to be reached to achieve adequate clearing of hydrated samples that still contain lipids.

Highly concentrated sugar or glycerol solutions can be difficult to work with due to their high viscosity. At the working concentrations required for index matching, there is potential for precipitation at room temperature, air bubbles can easily be introduced, and movement of the sample through the clearing solutions during imaging (see lightsheet imaging below) may not be possible. However, a number of alternative simple immersion clearing solutions with lower viscosities exist to avoid these issues. The proprietary FocusClear (Chiang et al., 2002) and recently published Refractive Index Matched solution (RIMs, Yang et al., 2014) utilize low-viscosity, high refractive index contrast reagents often used in biomedical imaging as their key components. Both diatrizoic acid (Hypaque) used in FocusClear and Histodenz used in RIMs are complex molecules that contain an aromatic ring and three iodine atoms (Figure 2D). This chemistry provides a large number of electrons for interaction with passing light waves (i.e., high refractive index) but in a relatively low-concentration, low-viscosity solution. In both cases, the high expense of these reagents may limit their use. Two lower-cost options are TDE and the FRUIT technique. TDE is a water-soluble, low-viscosity liquid that can be tuned over a range of refractive indices by diluting it in water. It was first demonstrated as a mounting media for super-resolution microscopy (Staudt et al., 2007) but can also clear large tissues (Aoyagi et al., 2015; Costantini et al., 2015). One drawback to TDE is that, at high concentrations, the brightness of a number of fluorophores is reduced (Staudt et al., 2007). FRUIT is a combination of the SeeDB and Sca*l*e (see below) techniques (Hou et al., 2015). FRUIT mixes urea with fructose to lower the overall viscosity of the SeeDB fructose solution and improve tissue penetration and clearing.

Although the techniques of passive clearing in simple aqueous solutions does not clear as well as the solvent-based methods or other aqueous-based clearing methods discussed below, they are economical and easy to implement and retain compatibility for use in samples with a wide range of florescent dyes and proteins, including lipid targeting dyes.

Hyperhydration

Most simple immersion techniques do not remove lipid and simply try to match the *average* refractive index of a tissue (>1.45) by replacing the liquid in and around a tissue with a high refractive index solution. An alternative approach is to remove lipid and reduce the refractive index of tissue samples during the clearing process. The first technique to take advantage of this mechanism was Sca*l*e (Hama et al., 2011). Sca*l*e utilizes detergent-based removal of lipid in conjunction with urea-mediated hydration (in the presence of glycerol) of the remaining tissue to produce a cleared sample (Figure 2C). The strategy to remove the lipid but without hydrophobic solvents (in order to maintain an aqueous environment for fluorescent proteins) is by extensive incubation lasting days to months with detergent (e.g., Triton X-100) and multiple solution changes. At the same time, urea is used to penetrate, partially denature, and thus hydrate even the hydrophobic regions of high refractive index proteins (Hua et al., 2008). This hyperhydration reduces the overall refractive index to ~1.38 (Hama et al., 2011). To our knowledge, the atomic-level explanation for this reduction in refractive index is not well understood. However, the reduced refractive index may be due to a spreading apart of dense, high refractive index scattering sites within protein complexes by partial denaturation and hydration. This view is supported by the observation that these samples have an expanded volume. This expansion can be controlled by adjusting glycerol levels in the clearing solution, which may act to lower the concentration of water that has access to protein moieties. If the relative placements or absolute sizes of objects in the tissue are important, then care must be taken, as greater hydration produces better clearing but also creates greater expansion. In addition, a larger sample will take longer to image. Interestingly, one recent approach that intentionally enlarges samples for the purpose of imaging diffraction-limited structures (see below) also has the effect of clearing the tissue.

ClearT, a simple immersion method that utilizes a urea-like molecule (formamide; Figure 2C) as the active clearing reagent, may partially act by this mechanism as well (Kuwajima et al., 2013). This potential hyperhydration may help to explain ClearT and FRUIT's ability to clear tissue thicker than most simple immersion techniques.

The urea-based CUBIC method utilizes a similar hyperhydration mechanism. However, a high refractive index sucrose-based clearing solution was proposed as an optional second step to expedite the clearing process (Susaki et al., 2014; Tainaka et al., 2014). CUBIC also uses very high triton levels (50%) to maximize lipid removal. This lipid removal process can result in a high degree of protein loss (24%–41%), which lowers epitope concentrations and potentially weakens immunostaining (Chung et al., 2013).

Hydrogel Embedding

The aqueous-based clearing methods discussed thus far are either limited to clearing small samples (simple immersion) or are slow (hyperhydration). In addition, any technique utilizing harsh solvents or high concentrations of detergent risks removal of large percentages of the protein content of the tissue. The CLARITY and PACT/PARS methods attempt to address these issues by first embedding the tissue in hydrogel (Chung et al., 2013; Tomer et al., 2014; Yang et al., 2014). After hydrogel embedding is complete, lipids are removed passively by a week(s)-long incubation in detergent (8% SDS) or rapidly (days) via electrophoresis. A final step of immersion in either FocusClear, the Histodenz-based clearing solution RIMs, TDE, or 80% glycerol produces a sample that is well cleared (Figure 2D).

The recent development of expansion microscopy, which synthesizes a hydrogel polymer network throughout a sample and then expands it by a factor of 4.5 times (essentially combining hyperhydration and hydrogel embedding), has demonstrated the role that hydration can play in clearing if the sample is embedded in hydrogel (Chen et al., 2015).

Methods suitable for Immunolabeling

A number of the techniques above have been shown to be compatible with immunolabeling protocols (Table 1). It should be noted, however, that immunolabeling steps should be performed prior to immersing samples in highly viscous final clearing solutions (e.g., FocusClear, CUBIC2, RIMs, high molarity sugar solutions, etc.), as the diffusion of antibodies will be hindered in these conditions. Additionally, very long incubation times (weeks/months) are required for antibodies to fully penetrate through large tissues. For this reason, protocols that embed tissues in large pore hydrogels are more likely to show rapid and complete immunolabeling (Yang et al., 2014). The use of single-domain antibodies (reviewed in Holliger and Hudson, 2005) or nucleic acid aptamers (reviewed in Bunka and Stockley, 2006), which are a fraction of the size of standard antibodies, can better access epitopes deep in a sample in a shorter period of time. Additionally, direct fluorophore conjugation to these probes reduces the need for two antibody incubation steps.

Finally, a new method termed eTANGO utilizes dynamic electric fields to move antibodies through large cleared tissue and ensure an even distribution of the label both spatially and temporally across the sample. Using this technique, an entire mouse brain can be stained within hours (K.H. Chung, personal communication).

Imaging Cleared Tissue

Advances in fluorescent light microscopy are at present happening at an astounding pace. A number of different optical sectioning techniques are commercially available, many of which are directly useful for imaging cleared tissue. These optical sectioning techniques include confocal, two-photon microscopy, and lightsheet fluorescence microscopy (LSFM; reviewed in Conchello and Lichtman, 2005; Mertz, 2011; Reynaud et al., 2008). Of these techniques, two-photon microscopy is best suited for imaging deep into non-cleared tissue. However, once light scatter is no longer a limiting factor, microscopists will need to reevaluate which fluorescence technique is best suited to their samples. Interestingly, cleared tissue imaging is now pushing the development of novel microscope technologies and components. Moreover, it is possible that certain labels that reflect light, such as the horseradish peroxidase (HRP), other peroxidase reaction products (e.g., APEX; Martell et al., 2012), or silver stains (e.g., the Golgi stain), might now be imaged in thicker volumes thanks to clearing. Thus, reflected light confocal (Boyde, 1985; Marques et al., 2000; Minsky, 1988) might make a comeback.

Working Distance in Confocal and Two-Photon Microscopy: Non-cleared Tissue

The working distance of an objective is the distance between its physical front lens and the point of focus within the sample. Confocal microscopes have a limited penetration depth of ~100–200 μm in non-cleared tissue. Therefore, most high numerical aperture (NA, a key determinant of resolution) objectives have been designed with working distances less than 200 μm. As NA and working distance are in general inversely proportional, most objectives that have working distances greater than 1 mm have lower resolving power, especially poor in the axial dimension.

Theoretical and experimental studies previously suggested that, in scattering tissue, 1 mm was approximately the depth limit of two-photon microscopy (Theer and Denk, 2006; Theer et al., 2003). When imaging this deep, scattering attenuates the excitation light that arrives at the point of focus. In addition, the volume of tissue illuminated by the hourglass-shaped laser beam rapidly increases as the point of focus moves deeper. Although the likelihood of two-photon excitation is low except at the point of focus, some two-photon excitation events can and do occur outside of this point. As a result, at a certain depth, fluorescence excitation events are as likely to occur away from the point of focus as within it. Because pinholes are not utilized in two-photon imaging, in and out of focus fluorescence emission are collected by the objective and imaged back onto the (non-descanned) detector. Therefore, at the maximum depth, out of focus fluorescence begins to dominate the image. Although a pinhole could be used to exclude fluorescence arising from scattering events outside the focal volume, at such depths, fluorescent light generated in the focal plane is highly scattered as it travels back through the sample to the objective. This scattered fluorescence light will then be rejected by the pinhole, reducing the signal to undetectable levels (Theer and Denk, 2006). Despite this physical limit, two-photon microscopy pushed design of objectives forward, as high-resolution objectives capable of imaging in the millimeter range were required. Primarily designed as water dipping objectives, the most important design element is a larger diameter front lens. The larger lens allows an objective to be designed with a 1–2 mm working distance while maintaining an NA of ~1.0.

Working Distance in Confocal and Two-Photon Microscopy: Cleared Tissue

Cleared tissue removes the penetration limits imposed by light scatter, meaning that objective working distance is most often the limiting factor in how deep a particular microscope can image. Early pioneers of cleared tissue imaging quickly discovered that imaging depth was no longer limited by their sample but by their objective. Therefore, initial publications featured images limited by virtue of being: (1) acquired at modest resolutions with long working distance low-NA objectives, (2) restricted to superficial regions with high-NA, high-magnification objectives, or (3) having to be imaged from both sides and fused into a single-volume stack in post-processing steps. Long working distance (>5 mm), high-NA (>0.9) objectives are now available from most microscope manufacturers and are the lenses of choice for cleared tissue imaging.

Interestingly, by clearing tissue, two-photon imaging at depths greater than 1 mm has now been realized. However, an obvious decrease in image quality can still be seen at points deep within the sample. Scattering of the emitted fluorescence light is greatly reduced in cleared tissue; however, some excitation still occurs outside the point of focus when using two-photon excitation deep within a sample (as discussed above). Therefore, the use of a physical pinhole in the return light path with cleared tissue two-photon imaging may improve image quality—hence, a hybrid confocal-two-photon microscope?

Confocal or Two-Photon?

Working distance and not light penetration is generally the limiting factor in the ability to image cleared tissue. Therefore, an upright microscope with large axial travel is essential for accommodating long working distance objectives and thick samples. However, two-photon excitation is often not necessary. In fact, in direct comparison, confocal imaging may produce better signal-to-noise ratios in certain samples due to the higher efficiency of one-photon excitation and a lower likelihood of cross-excitation in samples labeled with multiple dyes. In addition, multi-color confocal images can be acquired more quickly due to fast switching between laser lines (no tuning required). Two-photon imaging may still be advantageous for a number of situations, including imaging samples that were not completely cleared, preventing bleaching of out of focus planes while acquiring very large Z stacks, or exciting near UV fluorophores with IR light because even in cleared tissue short-wavelength light scatters to some degree. However, both confocal and two-photon methods require laser scanning, a time-consuming and slow process. In fact, scanning of an entire mouse brain with a volume of 1,000 mm^3 using a 20×/1.0 objective would require >4,200,000 images (assuming a 500 × 500 μm field of view and a 1 μm axial step size). At a relatively fast scan rate of 1 Hz, this would take nearly 50 days. Therefore, confocal and two-photon imaging of cleared tissue is only practical for high-resolution imaging of small, localized regions.

Lightsheet Imaging

Confocal and two-photon imaging techniques have a major limitation in the amount of time required to image a large sample. Therefore, the reinvention of lightsheet microscopy (originally described in 1903, awarded the Nobel Prize in 1925; Siedentopf and Zsigmondy, 1903) has been highly advantageous. Although the basic design of a lightsheet microscope—a thin plane of excitation light focused perpendicular to the axis of an imaging objective—is common to all lightsheet fluorescent microscopes, several different designs have arisen.

In all LSFM designs, a single plane, and only that plane, is illuminated by excitation light. This complete illumination removes the need to slowly raster scan a laser beam across the sample. Instead, an image of the entire plane can be captured on a camera in a single exposure. When combined with a fast scientific complementary metal-oxide semiconductor (sCMOS) camera, the readout speed, or the time it takes to move the sample to the next focal plane, becomes the limiting factor for temporal sampling. Speeds greater than 20 focal planes per second are easily achievable.

Unfortunately, there appears to be a tradeoff between the physical width of the lightsheet (which can determine the axial resolution) and the size of the volume that can be imaged. Techniques that project the thinnest lightsheets (5 to <1 μm) and hence provide the best axial resolution, including objective-coupled planar illumination microscopy (Holekamp et al., 2008), diSPIM (Wu et al., 2013), two-photon lightsheet (Planchon et al., 2011), Bessel beam lightsheet (Planchon et al., 2011), lattice lightsheet (Chen et al., 2014), and SCAPE (Bouchard et al., 2015), are limited to samples only a few hundreds of micrometers thick and comparably small in area.

Thicker lightsheets (4–40 μm), formed by cylindrical lenses coupled to low-NA focusing optics can be evenly projected over far greater areas (cm^2) and also allow deeper imaging (by preventing the steric hindrances that occur when using high NA excitation and imaging objectives). Lightsheet microscopes utilizing these designs are optimal for cleared tissue imaging when the highest optical resolution is not essential (Dodt et al., 2007; Susaki et al., 2014; Tomer et al., 2014; Verveer et al., 2007).

As with confocal and two-photon imaging, however, refractive index uniformity throughout the optical path is essential. If dipping objectives are used, these must be matched to the index of refraction of the clearing solution (see below).

Refractive Index Matching

Spherical aberration is a serious image degrading problem that occurs if the optics of the microscope are not accurately corrected for the various refractive indices that light transverses between the specimen plane and the objective. Light originating from a sample imbedded in a mounting medium may pass through a glass coverslip, air, or immersion media and finally encounter a number of glass/air interfaces throughout the objective and microscope body. Each interface of varying refractive index can cause blur in the final image. Objective designers take great care to adjust for all of these refractive index mismatches in the microscope's optics. However, as mentioned above, most long working distance objectives are designed for imaging in air or with water immersion (refractive index = 1.0 or 1.33, respectively). An objective that is incorrectly matched to the refractive index of the sample will not focus light to the correct point within the microscope. This will result in a high degree of spherical aberration. In addition, when using a refractive index mismatched objective, the optical focal plane will not move the same distance as the physical focus drive on the microscope, rendering measurements between points of interest in the final image unreliable (Hell et al., 1993). The commercially available long working distance, high-NA objectives already mentioned have been developed for use with many of the clearing agents discussed here. Some are manufactured for specific refractive index values, while others are tunable (via correction collar) over a wide range of indices.

Data Handling

In the example given above, it was estimated that >4,000,000 images would need to be acquired to cover a volume of 1,000 mm^3. This represents >30 TB of data per color channel (4 mega pixel camera, ~8 MB per image). This presents three challenges:

(1) how to write the data to storage media as it is acquired at rates in excess of 500 GB/hr, (2) where and how to store these massive data sets, and (3) how to analyze and process the data.

Big data is not unique to microscopy. Because of this, the computational infrastructure required to store and analyze image data of this scale does exist; although it is not inexpensive, the price of data storage is dramatically decreasing. Additionally, a number of commercial and open-source software packages now exist to assist researchers in dealing with this challenge.

Future Outlook

There can be little doubt that tissue clearing technologies will continue to evolve in the near future. While some of the recently published clearing techniques were developed serendipitously (Sca*l*e, ClearT), others were intentionally engineered. As the adoption of these approaches increases, it is likely that protocols, perhaps commercialized ones, will become available, removing much of the trial and error. New reagents that facilitate immunostaining in thick tissues such as aptamers and single-domain antibodies will also hopefully become widely available. In addition, a spate of new clearing-specific microscopes and objectives are sure to follow. One potentially exciting development is leveraging adaptive optics, a technique that has been widely used in astronomy to correct for atmospheric light scatter. This technology, which is typically based on a sensor to detect deformations in the return light's wavefront and corrects these via a deformable mirror or spatial light modulator, is now being applied to microscopy and is allowing for an extended depth penetration in non-cleared samples (Booth, 2007; Wang et al., 2014). Although adaptive optics alone do not seem to be able to produce crisp images at depths equivalent to those achievable with cleared tissue, when combined with the tissue clearing techniques described here, the achievable imaging depths and resolution would be potentially even greater (many centimeters).

In parallel with improved approaches to data acquisition, we must also meet the challenges of analyzing and comparing massive volumetric data sets to achieve statistically robust conclusions. With concerted and collaborative efforts along these lines, tissue clearing has the potential to open doors to many new discoveries and a more spatially integrated view of the inner workings of organisms.

ACKNOWLEDGMENTS

We are grateful to the Harvard Center for Biological Imaging for infrastructure and imaging support. J.W.L. is supported by NIMH Silvio Conte Center 1P50MH094271-010, NIH 1R01NS076467-01, DOD GG008784, NIH 1U01NS090449-01, NSF NIH Johns Hopkins University 2001668272, and HFSP RGP0051/2014.

REFERENCES

Alnuami, A.A., Zeedi, B., Qadri, S.M., and Ashraf, S.S. (2008). Oxyradical-induced GFP damage and loss of fluorescence. Int. J. Biol. Macromol. *43*, 182–186.

Aoyagi, Y., Kawakami, R., Osanai, H., Hibi, T., and Nemoto, T. (2015). A rapid optical clearing protocol using 2,2′-thiodiethanol for microscopic observation of fixed mouse brain. PLoS ONE *10*, e0116280.

Becker, K., Jährling, N., Saghafi, S., Weiler, R., and Dodt, H.U. (2012). Chemical clearing and dehydration of GFP expressing mouse brains. PLoS ONE *7*, e33916.

Booth, M.J. (2007). Adaptive optics in microscopy. Philos. Trans. A Math Phys. Eng. Sci. *365*, 2829–2843.

Bouchard, M.B., Voleti, V., Mendes, C.S., Lacefield, C., Grueber, W.B., Mann, R.S., Bruno, R.M., and Hillman, E.M. (2015). Swept confocally-aligned planar excitation (SCAPE) microscopy for high speed volumetric imaging of behaving organisms. Nat. Photonics *9*, 113–119.

Boyde, A. (1985). Stereoscopic images in confocal (tandem scanning) microscopy. Science *230*, 1270–1272.

Bunka, D.H., and Stockley, P.G. (2006). Aptamers come of age - at last. Nat. Rev. Microbiol. *4*, 588–596.

Cai, D., Cohen, K.B., Luo, T., Lichtman, J.W., and Sanes, J.R. (2013). Improved tools for the Brainbow toolbox. Nat. Methods *10*, 540–547.

Chalfie, M., Tu, Y., Euskirchen, G., Ward, W.W., and Prasher, D.C. (1994). Green fluorescent protein as a marker for gene expression. Science *263*, 802–805.

Chen, B.C., Legant, W.R., Wang, K., Shao, L., Milkie, D.E., Davidson, M.W., Janetopoulos, C., Wu, X.S., Hammer, J.A., 3rd, Liu, Z., et al. (2014). Lattice light-sheet microscopy: imaging molecules to embryos at high spatiotemporal resolution. Science *346*, 1257998.

Chen, F., Tillberg, P.W., and Boyden, E.S. (2015). Optical imaging. Expansion microscopy. Science *347*, 543–548.

Chiang, A.S., Lin, W.Y., Liu, H.P., Pszczolkowski, M.A., Fu, T.F., Chiu, S.L., and Holbrook, G.L. (2002). Insect NMDA receptors mediate juvenile hormone biosynthesis. Proc. Natl. Acad. Sci. USA *99*, 37–42.

Chung, K., Wallace, J., Kim, S.Y., Kalyanasundaram, S., Andalman, A.S., Davidson, T.J., Mirzabekov, J.J., Zalocusky, K.A., Mattis, J., Denisin, A.K., et al. (2013). Structural and molecular interrogation of intact biological systems. Nature *497*, 332–337.

Clancy, B., and Cauller, L.J. (1998). Reduction of background autofluorescence in brain sections following immersion in sodium borohydride. J. Neurosci. Methods *83*, 97–102.

Conchello, J.A., and Lichtman, J.W. (2005). Optical sectioning microscopy. Nat. Methods *2*, 920–931.

Costantini, I., Ghobril, J.P., Di Giovanna, A.P., Mascaro, A.L., Silvestri, L., Mullenbroich, M.C., Onofri, L., Conti, V., Vanzi, F., Sacconi, L., et al. (2015). A versatile clearing agent for multi-modal brain imaging. Sci. Reports *5*, 9808.

Denk, W., and Horstmann, H. (2004). Serial block-face scanning electron microscopy to reconstruct three-dimensional tissue nanostructure. PLoS Biol. *2*, e329.

Denk, W., Strickler, J.H., and Webb, W.W. (1990). Two-photon laser scanning fluorescence microscopy. Science *248*, 73–76.

Dodt, H.U., Leischner, U., Schierloh, A., Jährling, N., Mauch, C.P., Deininger, K., Deussing, J.M., Eder, M., Zieglgänsberger, W., and Becker, K. (2007). Ultramicroscopy: three-dimensional visualization of neuronal networks in the whole mouse brain. Nat. Methods *4*, 331–336.

Duong, H., and Han, M. (2013). A multispectral LED array for the reduction of background autofluorescence in brain tissue. J. Neurosci. Methods *220*, 46–54.

Ertürk, A., Becker, K., Jährling, N., Mauch, C.P., Hojer, C.D., Egen, J.G., Hellal, F., Bradke, F., Sheng, M., and Dodt, H.U. (2012a). Three-dimensional imaging of solvent-cleared organs using 3DISCO. Nat. Protoc. *7*, 1983–1995.

Ertürk, A., Mauch, C.P., Hellal, F., Förstner, F., Keck, T., Becker, K., Jährling, N., Steffens, H., Richter, M., Hübener, M., et al. (2012b). Three-dimensional imaging of the unsectioned adult spinal cord to assess axon regeneration and glial responses after injury. Nat. Med. *18*, 166–171.

Hama, H., Kurokawa, H., Kawano, H., Ando, R., Shimogori, T., Noda, H., Fukami, K., Sakaue-Sawano, A., and Miyawaki, A. (2011). Scale: a chemical approach for fluorescence imaging and reconstruction of transparent mouse brain. Nat. Neurosci. *14*, 1481–1488.

Hecht, E. (2001). Optics, Fourth Edition (Addison-Wesley).

Hell, S., Reiner, G., Cremer, C., and Stelzer, E.H.K. (1993). Aberrations in confocal fluorescence microscopy induced by mismatches in refractive index. J. Microsc. *169*, 391–405.

Holekamp, T.F., Turaga, D., and Holy, T.E. (2008). Fast three-dimensional fluorescence imaging of activity in neural populations by objective-coupled planar illumination microscopy. Neuron *57*, 661–672.

Holliger, P., and Hudson, P.J. (2005). Engineered antibody fragments and the rise of single domains. Nat. Biotechnol. *23*, 1126–1136.

Hong, G., Diao, S., Chang, J., Antaris, A.L., Chen, C., Zhang, B., Zhao, S., Atochin, D.N., Huang, P.L., Andreasson, K.I., et al. (2014). Through-skull fluorescence imaging of the brain in a new near-infrared window. Nat. Photonics *8*, 723–730.

Hou, B., Zhang, D., Zhao, S., Wei, M., Yang, Z., Wang, S., Wang, J., Zhang, X., Liu, B., Fan, L., et al. (2015). Scalable and DiI-compatible optical clearance of the mammalian brain. Front. Neuroanat. *9*, 19.

Hua, L., Zhou, R., Thirumalai, D., and Berne, B.J. (2008). Urea denaturation by stronger dispersion interactions with proteins than water implies a 2-stage unfolding. Proc. Natl. Acad. Sci. USA *105*, 16928–16933.

Ichimura, K., Miyazaki, N., Sadayama, S., Murata, K., Koike, M., Nakamura, K., Ohta, K., and Sakai, T. (2015). Three-dimensional architecture of podocytes revealed by block-face scanning electron microscopy. Sci. Rep. *5*, 8993.

Ke, M.T., Fujimoto, S., and Imai, T. (2013). SeeDB: a simple and morphology-preserving optical clearing agent for neuronal circuit reconstruction. Nat. Neurosci. *16*, 1154–1161.

Kuwajima, T., Sitko, A.A., Bhansali, P., Jurgens, C., Guido, W., and Mason, C. (2013). ClearT: a detergent- and solvent-free clearing method for neuronal and non-neuronal tissue. Development *140*, 1364–1368.

Lichtman, J.W., and Conchello, J.A. (2005). Fluorescence microscopy. Nat. Methods *2*, 910–919.

Marques, M.J., Conchello, J.A., and Lichtman, J.W. (2000). From plaque to pretzel: fold formation and acetylcholine receptor loss at the developing neuromuscular junction. J. Neurosci. *20*, 3663–3675.

Martell, J.D., Deerinck, T.J., Sancak, Y., Poulos, T.L., Mootha, V.K., Sosinsky, G.E., Ellisman, M.H., and Ting, A.Y. (2012). Engineered ascorbate peroxidase as a genetically encoded reporter for electron microscopy. Nat. Biotechnol. *30*, 1143–1148.

Meglinski, I.V., Bashkatov, A.N., Genian, E.A., Churmakov, D.Y., and Tuchin, V.V. (2002). The enhancement of confocal images of tissues at bulk optical immersion. Laser Phys. *13*, 63–69.

Mertz, J. (2011). Optical sectioning microscopy with planar or structured illumination. Nat. Methods *8*, 811–819.

Minsky, M. (1988). Memoir on inventing the confocal scanning microscope. Scanning *10*, 128–138.

Oh, S.W., Harris, J.A., Ng, L., Winslow, B., Cain, N., Mihalas, S., Wang, Q., Lau, C., Kuan, L., Henry, A.M., et al. (2014). A mesoscale connectome of the mouse brain. Nature *508*, 207–214.

Paez-Segala, M.G., Sun, M.G., Shtengel, G., Viswanathan, S., Baird, M.A., Macklin, J.J., Patel, R., Allen, J.R., Howe, E.S., Piszczek, G., et al. (2015). Nat. Methods *12*, 215–218.

Peters, W. (1961). Methoden zur Herstellung yon Aufhellungsverfahren. Zool. Anz. *167*, 233–240.

Planchon, T.A., Gao, L., Milkie, D.E., Davidson, M.W., Galbraith, J.A., Galbraith, C.G., and Betzig, E. (2011). Rapid three-dimensional isotropic imaging of living cells using Bessel beam plane illumination. Nat. Methods *8*, 417–423.

Renier, N., Wu, Z., Simon, D.J., Yang, J., Ariel, P., and Tessier-Lavigne, M. (2014). iDISCO: a simple, rapid method to immunolabel large tissue samples for volume imaging. Cell *159*, 896–910.

Reynaud, E.G., Krzic, U., Greger, K., and Stelzer, E.H. (2008). Light sheet-based fluorescence microscopy: more dimensions, more photons, and less photodamage. HFSP J. *2*, 266–275.

Rost, F.W.D. (1992). Fluorescence microscopy (Cambridge University Press).

Siedentopf, H., and Zsigmondy, R. (1903). Uber Sichtbarmachung und Groessenbestimmung ultramikroskopischer Teilchen, mit besonderer Anwendung auf Goldrubinglaesern. Annalen der Physik *10*, 1–39.

Spalteholz, W. (1898). Hand-atlas of human anatomy, Second Edition (J.B. Lippincott).

Spalteholz, W. (1914). Uber das Durchsichtigmachen von menschlichen und tierischen Praparaten (S. Hierzel).

Staudt, T., Lang, M.C., Medda, R., Engelhardt, J., and Hell, S.W. (2007). 2,2′-thiodiethanol: a new water soluble mounting medium for high resolution optical microscopy. Microsc. Res. Tech. *70*, 1–9.

Steinke, H., and Wolff, W. (2001). A modified Spalteholz technique with preservation of the histology. Ann. Anat. *183*, 91–95.

Susaki, E.A., Tainaka, K., Perrin, D., Kishino, F., Tawara, T., Watanabe, T.M., Yokoyama, C., Onoe, H., Eguchi, M., Yamaguchi, S., et al. (2014). Whole-brain imaging with single-cell resolution using chemical cocktails and computational analysis. Cell *157*, 726–739.

Tainaka, K., Kubota, S.I., Suyama, T.Q., Susaki, E.A., Perrin, D., Ukai-Tadenuma, M., Ukai, H., and Ueda, H.R. (2014). Whole-body imaging with single-cell resolution by tissue decolorization. Cell *159*, 911–924.

Theer, P., and Denk, W. (2006). On the fundamental imaging-depth limit in two-photon microscopy. J. Opt. Soc. Am. A Opt. Image Sci. Vis. *23*, 3139–3149.

Theer, P., Hasan, M.T., and Denk, W. (2003). Two-photon imaging to a depth of 1000 microm in living brains by use of a Ti:Al2O3 regenerative amplifier. Opt. Lett. *28*, 1022–1024.

Toga, A.W., Ambach, K.L., and Schluender, S. (1994). High-resolution anatomy from in situ human brain. Neuroimage *1*, 334–344.

Toga, A.W., Goldkorn, A., Ambach, K., Chao, K., Quinn, B.C., and Yao, P. (1997). Postmortem cryosectioning as an anatomic reference for human brain mapping. Comput. Med. Imaging Graph. *21*, 131–141.

Tomer, R., Ye, L., Hsueh, B., and Deisseroth, K. (2014). Advanced CLARITY for rapid and high-resolution imaging of intact tissues. Nat. Protoc. *9*, 1682–1697.

Tsai, P.S., Blinder, P., Migliori, B.J., Neev, J., Jin, Y., Squier, J.A., and Kleinfeld, D. (2009a). Plasma-mediated ablation: an optical tool for submicrometer surgery on neuronal and vascular systems. Curr. Opin. Biotechnol. *20*, 90–99.

Tsai, P.S., Kaufhold, J.P., Blinder, P., Friedman, B., Drew, P.J., Karten, H.J., Lyden, P.D., and Kleinfeld, D. (2009b). Correlations of neuronal and microvascular densities in murine cortex revealed by direct counting and colocalization of nuclei and vessels. J. Neurosci. *29*, 14553–14570.

Verveer, P.J., Swoger, J., Pampaloni, F., Greger, K., Marcello, M., and Stelzer, E.H. (2007). High-resolution three-dimensional imaging of large specimens with light sheet-based microscopy. Nat. Methods *4*, 311–313.

Wang, K., Milkie, D.E., Saxena, A., Engerer, P., Misgeld, T., Bronner, M.E., Mumm, J., and Betzig, E. (2014). Rapid adaptive optical recovery of optimal resolution over large volumes. Nat. Methods *11*, 625–628.

White, R.M., Sessa, A., Burke, C., Bowman, T., LeBlanc, J., Ceol, C., Bourque, C., Dovey, M., Goessling, W., Burns, C.E., and Zon, L.I. (2008). Transparent adult zebrafish as a tool for in vivo transplantation analysis. Cell Stem Cell *2*, 183–189.

Wu, Y., Wawrzusin, P., Senseney, J., Fischer, R.S., Christensen, R., Santella, A., York, A.G., Winter, P.W., Waterman, C.M., Bao, Z., et al. (2013). Spatially isotropic four-dimensional imaging with dual-view plane illumination microscopy. Nat. Biotechnol. *31*, 1032–1038.

Yang, B., Treweek, J.B., Kulkarni, R.P., Deverman, B.E., Chen, C.K., Lubeck, E., Shah, S., Cai, L., and Gradinaru, V. (2014). Single-cell phenotyping within transparent intact tissue through whole-body clearing. Cell *158*, 945–958.

Zimmermann, T. (2005). Spectral imaging and linear unmixing in light microscopy. Adv. Biochem. Eng. Biotechnol. *95*, 245–265.